Desalination and Water Treatment
www.deswater.com

doi: 10.5004/dwt.2017.20603

74 (2017) 354–361
May

Synthesis and photocatalytic application of nano La–Ce/TiO_2 composite catalyst

Ponnusamy Sivakumar*, Duraisamy Sudha, Ponnusamy Mahalingam, Andimuthu Loganathan

PG and Research Department of Chemistry, Arignar Anna Government Arts College, Namakkal 637002, Tamilnadu, India, Tel. +919865366488; email: shivagobi@yahoo.com (P. Sivakumar), Tel. +919443762195; email: dsudhajkm@gmail.com (D. Sudha), Tel. +919842864041; email: mahalinghamp@yahoo.com (P. Mahalingam), Tel. +919840952195; email: loghunadan@gmail.com (A. Loganathan)

Received 16 November 2016; Accepted 14 February 2017

ABSTRACT

Nano-sized TiO_2 photocatalyst co-doped with La and Ce (La–Ce/TiO_2) was prepared by sol–gel method, and it was characterized using X-ray diffraction (XRD), scanning electron microscopy with energy dispersive X-ray analysis and Fourier transform infrared spectroscopy. The XRD results confirmed the formation of anatase phase for the TiO_2 particles. The photocatalytic activity of the prepared catalyst was evaluated for the degradation of methylene blue (MB) under UV and visible light irradiations. The photodegradation of MB dye strongly dependent on the solution pH and catalyst load. The enhanced photodegradation of MB by La–Ce/TiO_2 followed the Langmuir–Hinshelwood (L–H) adsorption isotherm. The synthesized catalyst has better dye degradation under visible light when compared with UV light.

Keywords: Lanthanum; Cerium; Co-doping; Methylene blue; Kinetics

1. Introduction

The development of human society is affected by the two major problems namely the environmental pollution and energy crisis [1]. Among the two, environmental pollution is one of the greatest issues, which keep on increasing every year and causing irreparable damage to the earth. The photocatalytic technology using semiconductor materials is one of feasible route to minimize the above effects [2–5]. Semiconductor materials are mainly employed for photocatalytic reactions due to their favorable combination of electronic structure, light absorption properties, charge transport properties and greater excitation life time.

Various industries like textile dyeing, printing, paper, paint manufactures, etc., discharge significant quantities of synthetic organic dyes into the environment as effluent, which causes serious health problems. Biodegradation, adsorption and advanced oxidation processes are the processing techniques suggested for the removal of dyes from wastewater. The semiconductor acts as a photocatalyst for the light-induced photochemical reactions because of its unique characteristics of electronic structure by a filled valence band and an empty conduction band. The primary role of the semiconductor in photocatalysis is to absorb an incident photon, generate an electron–hole pair, facilitate its separation and transport within the system that should be followed by promoting both the oxidation and reduction reactions simultaneously [6].

The heterogeneous photocatalysis using TiO_2 as photocatalyst is the most attractive method. Here, an electron hole–pair is generated when the energy of an incident photon matches or exceeds the band gap energy of the semiconductor. Excited state conduction band electrons and valence band holes can recombine and dissipate the input energy as heat, and trapped in metastable surface states or react with electron donors and electron acceptors adsorbed on the surface of the semiconductor. The hole present in the valence band is a strong oxidant that can either oxidize or react with electron donors such as water or hydroxide ions to form hydroxyl radicals, which in turn react with pollutants, such as dyes, resulting in the mineralization of the most of the pollutants. Many studies resulted that the nanoparticles show some

* Corresponding author.

special photochemical characteristics when compared with the conventional larger particles [7]. Also, the band gap of the nanoparticles increases with the decrease of particle size [8]. The morphology, surface area, degree of crystallinity can be controlled by the preparation method and heat treatment [9].

Among numerous semiconductor materials TiO_2 are the most promising catalysts in photocatalysis, hydrogen generation and anode electrodes of photovoltaic cells because of their versatile properties in nature: biocompatible, clean, non-polluting, inexhaustible and its low cost [10]. However, the main disadvantage of using TiO_2 as a photocatalyst is that its band gap (3.2 eV for an anatase phase) lies in the near-UV range of the electromagnetic spectrum. The UV light could only create an electron–hole pairs and thereby initiate the process of photocatalysis. Thus, a serious research is going on to shift TiO_2 optical response to the visible light. To overcome this problem a numerous studies have been put forward for the enhancement of photocatalytic activity of TiO_2 by doping of different transition metal oxides such as Fe, Zn, Cu, Ni and V [11–13]. The band gap of TiO_2 for the photoexcitation thus reduces by doping of these metals, and simultaneously, the recombination rate of photogenerated electron–hole pair reduces.

Doping other ions in TiO_2 lattice has proven to be an efficient path to improve the photocatalytic activity [14–17]. TiO_2 showed enhanced photocatalytic activity when doping with rare earth ions and this can improve the separation efficiency of electron–hole pairs by trapping photogenerated electrons [18,19]. The preparation of modified TiO_2 nanoparticles by doping with different rare earth ions and the evaluation of its photocatalytic activity were very rarely reported in the literature. Moreover, the simultaneous doping of two different metals with TiO_2 has attracted a considerable attention. Therefore, in this work La and Ce co-doped TiO_2 photocatalyst (La–Ce/TiO_2) was prepared by sol–gel process, and the composite catalyst was used to investigate the photocatalytic degradation of methylene blue (MB) dye under UV and sunlight.

2. Experimental setup

2.1. Preparation of La–Ce/TiO_2

The La and Ce co-doped TiO_2 photocatalyst was prepared by sol–gel process as per the following procedure. About 17 mL of [$Ti(OBu)_4$] was dissolved in 22 mL of ethanol with constant stirring, and 1.5 mL of acetic acid was added dropwise to suppress the hydrolysis. The above solution was stirred for 30 min using a magnetic stirrer to get the solution A. Solution B was prepared by adding 22 mL of ethanol, 3.6 mL of water and each 10 mL of 0.1 M lanthanum nitrate and cerium nitrate. The solution B was slowly transferred to the solution A with constant stirring. The mixture was hydrolyzed at 25°C for about 30 min under agitation and a transparent sol was obtained. In order to complete the gelation, 24 h ageing was done at room temperature. The gel was dried at 100°C then milled to a powder and calcined for 3 h at a sintering temperature of 550°C.

2.2. Preparation of dye solution

MB a cationic dye with a molecular formula of $C_{16}H_{18}ClN_3S.2H_2O$, molecular weight: 319, C.I. No. 52015 and

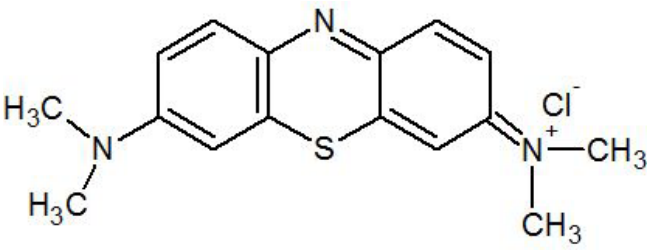

Fig. 1. Structure of methylene blue.

λ max: 640 nm (E. Merck, India) was used for the photocatalytic degradation studies. A stock solution of 1,000 mg/L was prepared by dissolving 1,000 mg of MB dye in 1.0 L of double-distilled water. The stock solution was diluted with double-distilled water to prepare the diluted solutions as and when required. The structure of MB is shown in Fig. 1.

2.3. Adsorption studies

The adsorption experiments were carried out in 250 mL tight lid reagent bottle (Borosil-R) by agitating 40 mg of adsorbent with 100 mL of the aqueous dye solution. The contents of the flasks were agitated by placing them in a temperature controlled orbital shaker (Remi). The mixture was withdrawn at specified interval, and then centrifuged using electrical centrifuge (Universal) at 5,000 rpm for 5 min. Double beam UV–Vis spectrometer (Systronics, model: 2201) was used to measure the final concentration of the dye solution by measuring the absorbance at the 640 nm (λ max of MB dye). The pH of the adsorptive solution was adjusted using 0.1 N NaOH and 0.1 N HCl for the studies of pH effect. Except for the effect of pH, all the other experiments were carried out at the pH of 8.0 (i.e., the original pH dye solution).

2.4. Photocatalytic studies

The photocatalytic degradation study of the dye solution was done in an annular type photoreactor, in which a central lamp was surrounded by 16 reaction cells. Light source of high-pressure mercury vapor lamp (160 W, 210–240 V Philips, India) at the central axis was used for the generation of UV radiation with a wavelength of $\lambda \geq 365$ nm. Similarly, the photocatalysis under visible radiation is carried out using a photoreactor made of tungsten filament lamp (60 W, 210–240 V Philips, India) at the central axis surrounded by 16 reaction cells made up of borosilicate glass. The reaction cells with a capacity of 110 mL are made of Pyrex tubes. During irradiation the contents present in the reaction cells are continuously stirred using magnetic stirrer. The schematic representation of the photoreactor is shown in Fig. 2.

La–Ce/TiO_2 photocatalyst of known quantity was added to 100 mL of MB solution of specified concentration in the sampling tube. The temperature of the reaction was maintained at 30°C ± 3°C (room temperature) for all the experiments, and the system was irradiated with a light source. For a particular time interval, the sample tube was removed from the slot, centrifuged using Universal-make centrifuge at 5,000 rpm for 5 min, and the final concentration was determined using UV–Vis spectrometer as stated in section 2.3.

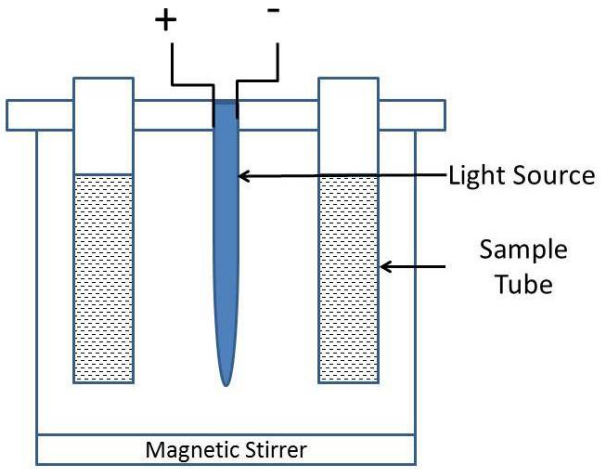

Fig. 2. The schematic representation of the photoreactor.

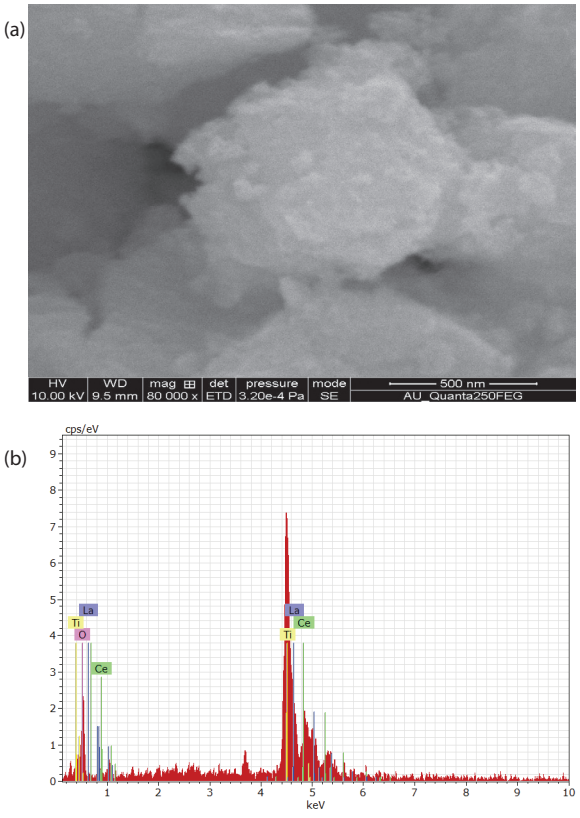

Fig. 3. (a) SEM images of La–Ce/TiO_2 photocatalyst. (b) EDXA spectra of La–Ce/TiO_2 catalyst.

2.5. Characterization studies

The scanning electron microscope (SEM) images were observed using QUANTA 250 FEG field emission SEM. The X-ray diffraction (XRD) patterns were studied by X-ray diffractometer with Cu Kα radiation, operated at 40 kV and 30 mA. Fourier transform infrared (FTIR) spectra were recorded using Thermo Nicolet FTIR spectrometer in ATR mode in the range of 400–4,000 cm^{-1}.

2.6. Point of zero charge

One gram of catalyst was mixed with 50 mL of sodium nitrate solution of an approximate concentration of 0.01 M in 10 numbers of 100 mL beakers. The suspensions were adjusted to various pH values with dilute sodium hydroxide and nitric acid solutions. After 60 min for equilibration, the initial pH values were measured. Then 1 g of sodium nitrate was added to each suspension to adjust the final electrolyte concentration to about 0.45 M. After an additional 60 min agitation, the final pH was measured. The difference between the final pH and initial pH (final pH – initial pH) was plotted against final pH. The point of zero pH indicates the point of zero charge pH.

3. Results and discussion

3.1. Characteristics of La–Ce/TiO_2 photocatalyst

The SEM images in conjunction with energy dispersive X-ray analysis (EDXA) analysis were utilized to interpret the results of the structure morphology and elemental composition. The SEM images of La–Ce/TiO_2 photocatalyst are shown in Fig. 3(a). The SEM images indicated that the rare earth metal doped catalyst has crystalline structure along with some irregularly shaped morphology. The particle agglomeration leads to more crystalline structures because of high temperature sintering. This irregularly shaped morphology is formed by means of a highly active agglomerated particle during sintering at a temperature of 550°C. These sintered nanocrystalline particles are further used for the dye degradation studies.

The EDXA was performed to confirm the composition of the prepared composite catalyst and the spectrum showed in Fig. 3(b). From the figures, the peaks correspond to oxygen, titanium, lanthanum and cerium elements inferring that the sample contains only the above said elements confirm the purity of grown material without any additive impurities. The elemental composition of the sample is given in Table 1. The elemental composition indicates that the prepared catalyst is pure and is synthesized as expected based on the reactants.

Fig. 4 shows the XRD pattern of La^{3+} and Ce^{3+} on the phase composition of La–Ce/TiO_2 catalyst. As observed from Fig. 4, the peaks at 25.28°, 38.18°, 48.44°, 53.90°, 62.64° and

Table 1
The elemental composition of the La–Ce/TiO_2 catalyst

Element	Atomic number	Series (wt%)	unn. C (wt%)	norm. C (at%)	Atom. C (wt%)	Error (1 sigma)
O	8	K	31.62	42.23	76.60	10.71
Ti	22	K	21.40	28.58	17.33	0.84
La	57	L	13.16	17.57	3.67	0.63
Ce	58	L	8.70	11.62	2.41	0.49

75.22° elucidate the diffraction patterns of (101), (112), (200), (105), (204) and (215) planes of anatase–TiO_2 which could be indexed as the anatase phase (PDF 21-1272). From XRD patterns, it was inferred that the co-doped catalyst La–Ce/TiO_2 has the anatase crystalline phase.

The crystalline phase of titania plays an important role to determine the photocatalytic activity. Thus, the dopant is expected to show an important role in the selective crystallization of anatase phase in sol–gel process [20]. The anatase form of TiO_2 exhibit more photocatalytic activity than the rutile phase. Also, the anatase phase showed low rate of recombination than rutile phase due to its tenfold greater rate of hole trapping [21].

The surface chemical bonding state of the prepared sample was characterized by FTIR spectroscopy as shown in Fig. 5. The spectra showed vibration band at 800–1,200 cm^{-1} corresponding to the O–Ti–O bonding [22]. A broad band near 3,400 cm^{-1} corresponds to the existence of water molecules and large number of hydroxyl groups adsorbed on the surfaces [23]. The peak at 1,650 cm^{-1} showed the O–H bending vibrations of adsorbed water molecules [24].

3.2. Adsorption of MB by La–Ce/TiO_2 photocatalyst

Sorption of the dye molecule is an important factor to determine the rate of photocatalytic degradation. An electron donor produced by the adsorption of dye on the surface of the semiconductor particles promotes an electron from its excited state to the conduction band of the semiconductor under UV irradiation. Here, adsorption in dark was carried out for various concentrations to evaluate the equilibrium constants of the adsorption of the dye on the surface of the photocatalyst. Fig. 6 shows an isotherm of L-shape based on the classification of Giles et al. [25]. From the L-shape of the isotherm, it is revealed that no strong competition between the solvent and the adsorbate to the surface sites of the adsorbent [26].

The adsorption of MB on to La–Ce/TiO_2 was studied at different initial concentrations at room temperature. The prepared photocatalyst may have adsorption capacity toward the dye molecule along with photocatalysis as the catalyst is in nanosize and it has more surface area. To get an idea about the real photocatalytic activity of the prepared sample, it is important to subtract the adsorption capacity of the sample. The rate of removal of dye molecule with respect to irradiation time at various initial dye concentrations is shown in Fig. 6. The adsorption was rapid at the beginning and it slowly decreased in the midway and finally reached equilibrium at 50 min. The increase in initial dye concentration also increases the amount of MB adsorbed per gram of the adsorbent. Though the catalyst composite shows the little amount of adsorption, the photocatalytic degradation seems to be the greater mode of dye removal.

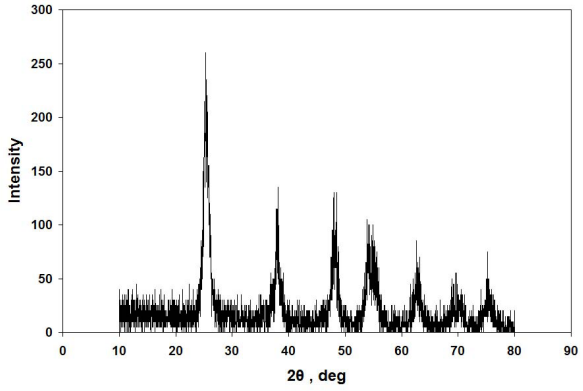

Fig. 4. XRD of La–Ce/TiO_2 catalyst.

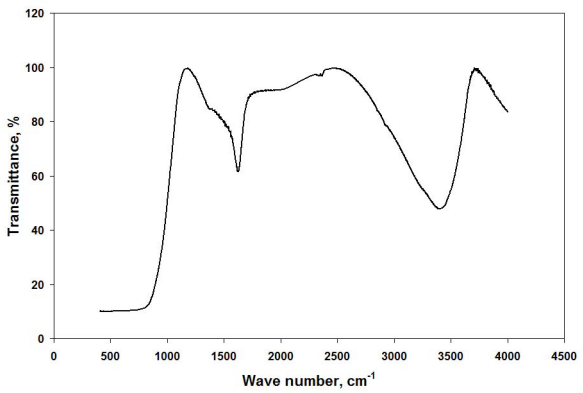

Fig. 5. FTIR spectra of La–Ce/TiO_2 catalyst.

3.3. Effect of pH on MB degradation

Solution pH is one of the major factors which control the rate of photocatalytic decomposition of organic molecules [27]. Large scale treatment of dye bearing wastewater requires a proper control of pH in order to ensure high efficiency and more economic benefits.

The photodegradation of MB dye using La–Ce/TiO_2 composite catalyst was performed at a pH range of 2–10. The variation of MB degradation with respect to pH is shown in Fig. 7. The photocatalytic decomposition of MB increases with increase of pH. The maximum degradation was observed at basic pH. The zero point charge of La–Ce/TiO_2 composite is 6.8, and the surface of the catalyst is negative when the pH goes above 7.2. The MB dye will exists as $[MB]^+$ at basic pH.

$$[MB–Cl] \rightarrow [MB]^+ + Cl^-$$

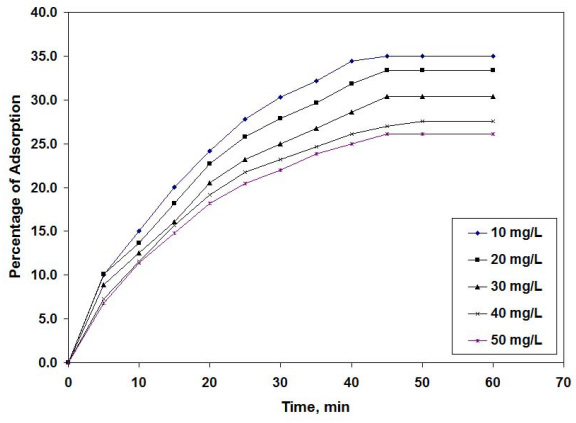

Fig. 6. Adsorption of MB by La–Ce/TiO_2 catalyst.

The negative surface of the catalyst will attract the positively charged $[MB]^+$ ions and because of that the photocatalytic degradation of $[MB]^+$ induced more. Another possible pathway is that at high pH the OH^- ions present in the solution will combine with the holes of the catalyst and produces more $OH^\bullet$ radicals [28]. As the hydroxyl radicals are dominant species which will favor the fast decomposition of $[MB]^+$ ions into smaller fragments.

The possible cause for the lower degradation at the lower pH is that the Cl^- ions present in the dye molecule may reduce the activity of the La–Ce/TiO_2 catalyst. Based on the following three possible pathways reported by the previous researchers, Cl^- ion plays a negative role on the decomposition of MB dye at lower pH.

- At the acidic pH, the catalyst surface exists as $[La–Ce/TiO_2]^+$. Thus, the positively charged catalyst surface will attract the Cl^- ions of (MB dye) and ultimately minimizes the available surface area as well as active sites and thereby the degradation efficiency is reduced [29].
- Another possible reason is that at lower pH, the Cl^- acts as electron scavengers competing with the molecular oxygen and prevents the formation of $OH^\bullet$ radicals. Therefore, the formation of super oxide followed by $OH^\bullet$ formation is prevented [30].
- The third possible reason is that the formed free radicals are scavenged by Cl^- through some additional reactions. This reduction in free radical concentration reduces the photodegradation of MB [31].

Based on the studies on the effect of pH, the optimum pH for further photodegradation studies was fixed as 8.0.

3.4. Effect of catalyst load

The first and foremost objective is to optimize the amount of catalyst required for the effective oxidative degradation of MB by La–Ce/TiO_2 composite. Here, the experiments were carried out by varying catalyst load between 5 and 50 mg with 100 mL of the dye solution of 40 mg/L concentration at a pH of 8.0. The optimization of catalyst loading was done by keeping the contents under respective light for 3 h, and the final concentration of the dye solution was determined spectrophotometrically after removing the catalyst by centrifugation. The variation in MB degradation as a function of catalyst dosage under UV and visible light are shown in Fig. 8.

It was observed that the amount of dye degradation increased with increasing the catalyst load from 5 to 40 mg. When the catalyst load exceeds 40 mg the amount of dye degraded under UV and visible light show a slight decrease. The decrease in photodegradation at a catalyst loading of above 40 mg was due to the fact that the excess catalyst prevents the effective light absorption and there by decreases the photodegradation [32]. Hence, 40 mg catalyst load for 100 mL was fixed as the optimum dosage for further photodegradation studies. Also, the optimal concentration of catalyst depends on working conditions, surface area of the catalyst and wavelength of the incident radiation [33,34].

3.5. Kinetic studies of the photodegradation

In order to employ the photocatalytic process for the elimination of organic pollutants present in the wastewater, it is essential to have a sound knowledge about the kinetics and mechanism of the decomposition process. Pseudo-first order, pseudo-second order and Langmuir–Hinshelwood kinetic expressions were widely used by majority of the researchers today to describe the photocatalytic oxidation of organic compounds [35]. Pseudo-first-order kinetics is a special form of L–H kinetics [36]. According to the literature review, the dependence of photocatalytic degradation rates on the concentration of organic pollutants has been well represented by Langmuir–Hinshelwood (L–H) kinetic model. The modified equation of L–H is given by [37]:

$$r = \frac{-dC}{dt} = k_r\theta = k_r KC / 1 + KC \quad (1)$$

where k_r is the reaction rate constant, θ is the fraction of TiO_2 surface coverage, K is the reactant adsorption constant and C is the concentration of substrate at a time of t.

During the photocatalytic degradation of complex organic molecules, many intermediates are formed and this may interfere in the determination of kinetic owing to the

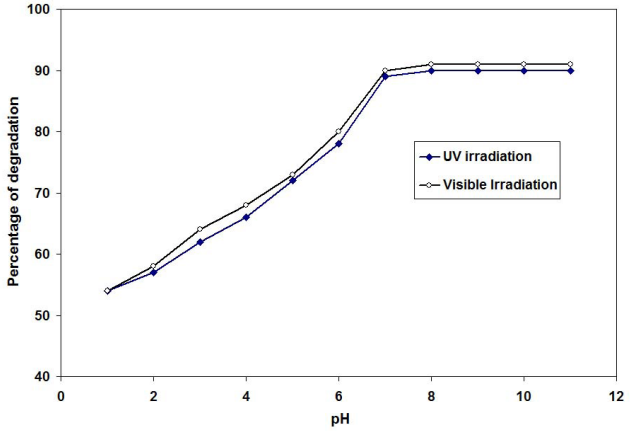

Fig. 7. Effect of pH for the photodegradation of MB by La–Ce/TiO_2.

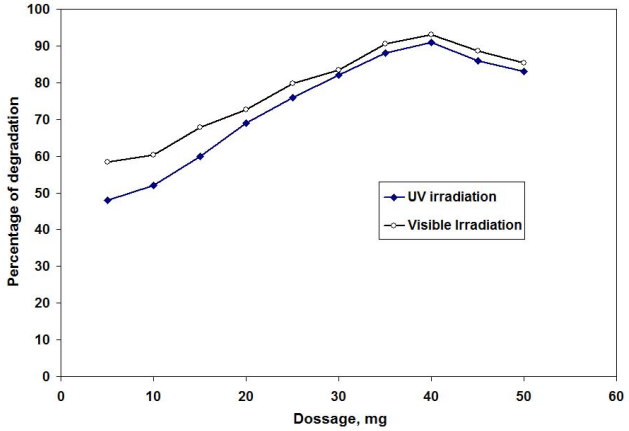

Fig. 8. Effect of catalyst load for the photodegradation of MB by La–Ce/TiO_2.

competitive adsorption and degradation [37]. To minimize impacts caused by the competitive adsorption and degradation products, it is essential to consider the initial rate of degradation for the kinetic studies. Based on this consideration, the photocatalytic degradation rate as a function of concentration can be expressed as:

$$r_0 = k_r K C_0 / 1 + K C_0 \quad (2)$$

where r_0 is the initial rate of photocatalytic degradation of MB and C_0 is the initial concentration of the dye solution. During the photocatalytic degradation of complex organic molecules, when the substrate concentration is low, the surface of the photocatalyst will not be saturated. In such conditions, the photocatalytic degradation of the dye molecule (MB in this study) with catalyst follows apparent first-order kinetics [37]. Based on the assumption of apparent first-order kinetics, Eq. (2) is modified as:

$$\ln\left(\frac{C_0}{C}\right) = k_r K_t = k_{app} t \quad (3)$$

where $k_{app} = k_r K$.

Here, the slope of linear variations equal to the k_{app}, the apparent first-order rate constant, and it was determined from the slope of the plot $\ln(C_0/C)$ vs. time is shown in Figs. 9(a) and (b). The figures showed that the photocatalytic degradation follows the pseudo-first-order kinetic with respect to MB concentrations.

The kinetic studies results for both UV and solar irradiations are presented in Table 2.

The kinetic studies are done initially with the dye concentration of 10 mg/L up to 50 mg/L with the catalytic dosage is fixed as 20 mg/50 mL of the dye solution. The dye degradation studies under UV and solar are carried out with the time interval of 5 min till 1 h at a pH range of 2–10. Here, when increasing the initial concentration of MB from 10 to 50 mg/L, the apparent rate constant for the photodegradation of MB by La–Ce/TiO_2 decreases from 7.95 × 10^{-2} to 2.95 × 10^{-2} min^{-1} under UV irradiation and it decreases from 9.65 × 10^{-2} to 3.14 × 10^{-2} min^{-1} for solar irradiation. The decrease of the rate constant on increasing the initial dye concentration substantiates that more intermediate formation and competitive adsorption started to operate during the concentration increases. From the above results, the lower MB concentration shows better agreement with the first-order reaction.

The plot of initial rate (r_0) of the MB degradation vs. initial dye concentration is shown in Fig. 10. As observed from Fig. 10, the rate of MB degradation showed a sharp increase with increasing the initial MB concentration and at higher MB concentration it finds an independent behavior.

The following expression obtained by the inverse of Eq. (2) gives the dependence of $1/r_0$ values on the appropriate $1/C_0$ values of MB concentration:

$$\frac{1}{r_0} = \frac{1}{k_r} + \frac{1}{k_r K}\frac{1}{C_0} \quad (4)$$

The above variation is represented in Fig. 11. The figure showed a linear variation confirming the Langmuir–Hinshelwood relationship to the initial rate of photodegradation. The calculated values of k_r and K from the intercept and slope of the straight line for UV radiation were (r^2 = 0.9957) 0.066 mg/L:62.90 L/mg. Similarly, for solar radiations the values were (R^2 = 0.9929) 0.060 mg/L:142.73 L/mg, respectively.

Thus, the photocatalytic decomposition of MB by La–Ce/TiO_2 photocatalyst obeyed first-order kinetics under UV and solar irradiation with good correlation coefficient.

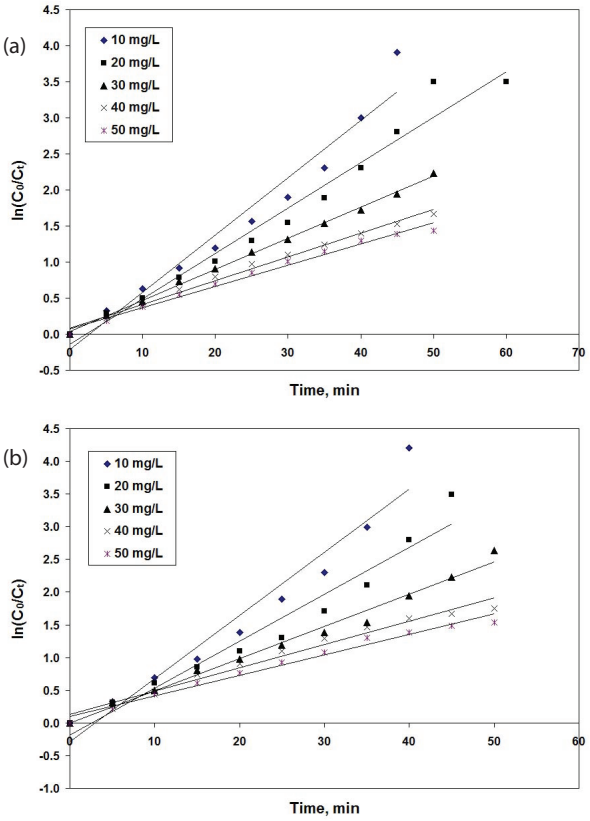

Fig. 9. Plot of $\ln(C_0/C)$ vs. time for the photodegradation of MB by La–Ce/TiO_2: (a) UV irradiation and (b) visible irradiation.

Table 2
Photodegradation kinetic results of MB by La–Ce/TiO_2 photocatalyst

Irradiation light	Initial dye concentration, mg/L	k_{app} × 10^{-2}, min^{-1}	r^2
UV light	10	7.95	0.9560
	20	6.30	0.9739
	30	4.31	0.9983
	40	3.29	0.9922
	50	2.95	0.9874
Solar light	10	9.65	0.9495
	20	7.17	0.9538
	30	4.93	0.9875
	40	3.56	0.9773
	50	3.14	0.9826

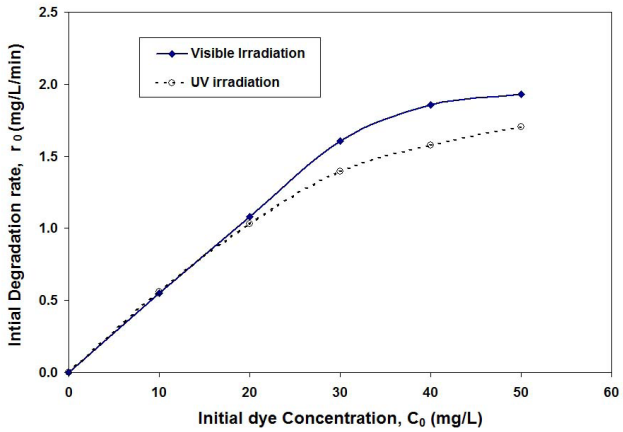

Fig. 10. Plot of initial rate (r_0) vs. initial dye concentration (C_0).

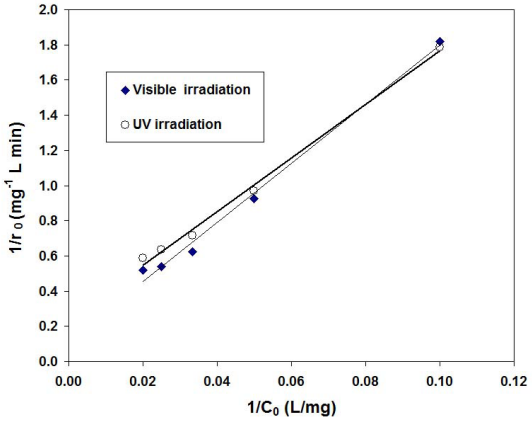

Fig. 11. L–H plot for the photodegradation of MB by La–Ce/TiO_2.

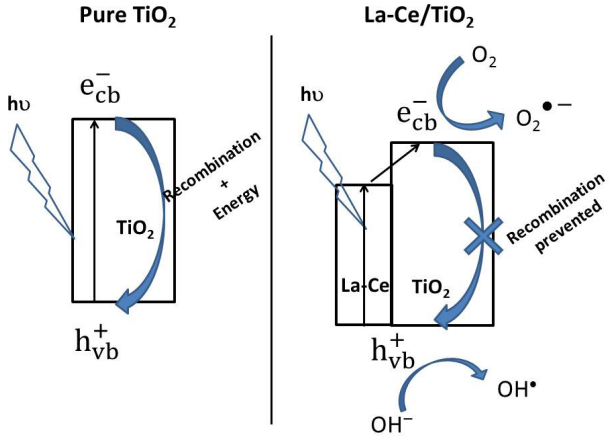

Fig. 12. Mechanism of photodegradation.

3.6. Mechanism of photodegradation

On comparing the degradation rate of MB dye without catalyst (photolysis) and with catalyst (photocatalysis), the degradation rate improved to a greater extent when the composite catalyst is added. Among the photocatalysis using UV and solar irradiations, solar light proved to be more efficient than UV light. The most activity of the composite catalyst is due to the well known reason that when La–Ce/TiO_2 is irradiated with light, the electrons are promoted from the valance band to the conduction band of the catalyst leading to the formation of an electron–hole pair (Fig. 12).

$$La–Ce/TiO_2 + h\nu \rightarrow La–Ce/TiO_2\ (e^-_{CB} + h^+_{VB})$$

The valence band potential (h^+_{VB}) is positive enough to generate hydroxyl radical from hydroxyl ions and the oxygen molecules are reduced by the negative potential of the conduction band (e^-_{CB}) [37].

The hydroxyl radical generated by the catalyst acts as a powerful oxidizing agent and attacks the MB present on the surface of the catalyst. The reaction gradient decreases when the distance from the catalyst surface increases toward the bulk of the solution.

$$h^+_{VB} + e^-_{CB} \rightarrow \text{recombination} + \text{energy}$$

The most frequent occurrence of electron–hole recombination is minimized by doping with La–Ce. The La–Ce also acts as a sensitizer and enhances the generation of electron–hole pair and prevents the recombination. The electron and the hole generated by the irradiation generated hydroxide and oxide ion radicals as per the following sequence.

$$h^+_{VB} + OH^- \rightarrow OH^{\bullet} e^- + O_2 \rightarrow O_2^{\bullet -}$$

The generated hydroxyl radicals are responsible for the photodegradation of MB dye.

$$OH^{\bullet} + MB \rightarrow \text{oxidized products}$$

4. Conclusions

The La, Ce co-doped titania composite (La–Ce/TiO_2) photocatalyst synthesized by this study is found to have anatase form with 50–100 nm size. The prepared photocatalyst is effective under UV and solar radiations. The irregularly shaped morphology was observed from SEM analysis and these are formed by means of a highly active agglomerated particle during sintering. The FTIR spectra showed a vibration band at 800–1,200 cm^{-1} are the characteristics of O–Ti–O network. The photocatalytic activity of MB by La–Ce/TiO_2 was high under alkaline conditions. The degradation follows the pseudo-first-order kinetics based on the analysis with modified Langmuir–Hinshelwood model. Therefore, the La–Ce/TiO_2 photocatalyst is a promising material for the degradation of organic dyes under UV and solar irradiations.

Acknowledgment

The author Dr. P. Sivakumar thank UGC-SERO, Hyderabad for the financial assistance under Minor Research Project (P. No: 1942) Scheme.

References

[1] C.Y. Lin, C.H. Lay, B. Sen, C.Y. Chu, G. Kumar, C.C. Chen, Fermentative hydrogen production from wastewaters: a review and prognosis, Int. J. Hydrogen Energy, 37 (2012) 15632–15642.

[2] J.H. Wu, J.L. Wang, J.M. Lin, Z. Lan, Q.W. Tang, M.L. Huang, Y.F. Huang, L.Q. Fan, Q.B. Li, Z.Y. Tang, Gd–La codoped TiO_2 nanoparticles as solar photocatalysts, Adv. Energy Mater., 2 (2012) 78–81.

[3] L. Pan, J.J. Zou, X.W. Zhang, L. Wang, Water-mediated promotion of dye sensitization of TiO_2 under visible light, J. Am. Chem. Soc., 133 (2011) 10000–10002.

[4] Z.J. Gu, Y.C. Yang, K.Y. Li, X.Y. Tao, G. Eres, J.Y. Howe, L.T. Zhang, X.D. Li, Z.W. Pan, Aligned carbon nanotube-reinforced silicon carbide composites produced by chemical vapor infiltration, Carbon, 49 (2011) 2475–2482.

[5] H. Zhou, X.F. Li, T.X. Fan, F.E. Osterloh, J. Ding, E.M. Sabio, D. Zhang, Q.X. Guo, Artificial inorganic leafs for efficient photochemical hydrogen production inspired by natural photosynthesis, Adv. Mater., 22 (2010) 951–956.

[6] L.M. Peter, Dye-sensitized nanocrystalline solar cells, Phys. Chem. Chem. Phys., 9 (2007) 2630–2642.

[7] T. Torimoto, H. Kontani, Y. Shibutani, S. Kuwabata, T. Sakata, H. Mori, H. Yoneyama, Characterization of ultra small CdS nanoparticles prepared by the size-selective photo etching technique, J. Phys. Chem. B, 105 (2001) 6838–6845.

[8] M. Addamo, V. Augugliaro, A. Di Paola, E. Garcıa-Lpez, V. Loddo, G. Marcı, R. Molinari, L. Palmisano, M. Schiavello, Preparation, characterization, and photoactivity of polycrystalline nanostructured TiO_2 catalysts, J. Phys. Chem. B, 108 (2004) 3303–3310.

[9] D. Bersani, G. Antonioli, P.P. Lottici, T. Lopez, Raman study of nanosized titania prepared by sol–gel route, J. Non-Cryst. Solids, 232–234 (1998) 175–218.

[10] J.H. Park, S. Kim, A.J. Bard, Novel carbon-doped TiO_2 nanotube arrays with high aspect ratios for efficient solar water splitting, Nano Lett., 6 (2006) 24–28.

[11] S. Penner, Steps toward the hydrogen economy, Energy, 31 (2006) 33–43.

[12] H.J. Choi, M. Kang, New and future developments in catalysis: solar photocatalysis, Int. J. Hydrogen Energy, 32 (2007) 3841–3848.

[13] L.S. Yoong, F.K. Chong, B.K. Dutta, Development of copper-doped TiO_2 photocatalyst for hydrogen production under visible light, Energy, 34 (2009) 1652–1661.

[14] A.R. Gandhe, J.B. Fernandes, A simple method to synthesize N-doped rutile titania with enhanced photocatalytic activity in sunlight, J. Solid State Chem., 178 (2005) 2953–2957.

[15] D. Chatterjee, S. Dasgupta, Visible light induced photocatalytic degradation of organic pollutants, J. Photochem. Photobiol., C, 6 (2005) 186–205.

[16] D. Masih, H. Yoshitake, Y. Izumi, Photo-oxidation of ethanol on mesoporous vanadium–titanium oxide catalysts and the relation to vanadium(IV) and (V) sites, Appl. Catal., A, 325 (2007) 276–282.

[17] M.M. Mohamed, M.M. Al-Esaimi, Characterization, adsorption and photocatalytic activity of vanadium-doped TiO_2 and sulfated TiO_2 (rutile) catalysts: degradation of methylene blue dye, J. Mol. Catal. A: Chem., 255 (2006) 53–61.

[18] K.T. Ranjit, I. Willner, S.H. Bossmann, A.M. Braun, Lanthanide oxide-doped titanium dioxide photocatalysts: novel photocatalysts for the enhanced degradation of *p*-chloro phenoxyacetic acid, Environ. Sci. Technol., 35 (2001) 1544–1549.

[19] J.C. Gacon, K. Horchani, A. Jouini, C. Dujardin, I. Kamenskikh, Optical properties of praseodymium concentrated phosphates, Opt. Mater., 28 (2006) 14–20.

[20] M. Hirano, C. Nakahara, K. Ota, M. Inagaki, Direct formation of zirconia-doped titania with stable anatase-type structure by thermal hydrolysis, J. Am. Ceram. Soc., 85 (2002) 1333–1335.

[21] S. Sakthivel, M.C. Hidalgo, D.W. Bahnemann, S.U. Geissen, V. Murugesan, A. Vogelpohl, A fine route to tune the photocatalytic activity of TiO_2, Appl. Catal., B, 63 (2006) 31–40.

[22] G. Shao, X. Zhang, Z. Yuan, Preparation and photocatalytic of hierarchically mesoporous-macroporous $TiO_{2-x}N_x$, Appl. Catal., B, 82 (2008) 208–218.

[23] Z. Ding, G.Q. Lu, P.F. Greenfield, Role of the crystalline phase of TiO_2 in heterogeneous photocatalysis for phenol oxidation in water, J. Phys. Chem. B, 104 (2000) 4815–4820.

[24] C. Deng, F.P. James, V.P. Wright, Poly(tetraethylene glycol malonate)–titanium oxide hybrid materials by sol-gel methods, J. Mater. Chem., 8 (1998) 153–159.

[25] C.H. Giles, A.P. D'Silva, I.A. Easton, A general treatment and classification of the solute adsorption isotherm part. II. Experimental interpretation, J. Colloid. Interface Sci., 47 (1974) 766–778.

[26] N. Barka, S. Qourzal, A. Assabbane, A. Nounah, Y. Ait-Ichou, Photocatalytic degradation of an azo reactive dye, ReactiveYellow 84 in water using an industrial titanium dioxide coated media, Arab. J. Chem., 3 (2010) 279–283.

[27] P. Velusamy, S. Pitchaimuthu, S. Rajalakshmi, N. Kannan, Modification of the photocatalytic activity of TiO_2 by β-cyclodextrin in decoloration of ethyl violet dye, J. Adv. Res., 5 (2014) 19–25.

[28] S. Kaneco, M.A. Rahman, T. Suzuki, H. Katsumata, K. Ohta, Optimization of solar photocatalytic degradation conditions of bisphenol in water using titanium dioxide, J. Photochem. Photobiol., A, 163 (2004) 419–424.

[29] K. Wang, Y.H. Hsieh, M.Y. Chou, C.Y. Chang, Photocatalytic degradation of 2-chloro and 2-nitrophenol by titanium dioxide suspensions in aqueous solution, Appl. Catal., B, 21 (1999) 1–8.

[30] J.M. Tseng, C.P. Huang, Removal of chlorophenols from water by photocatalytic oxidation, Water Sci. Technol., 23 (1991) 377–387.

[31] M. Abdullah, G.K. Low, R.W. Matthews, Effects of common inorganic anions on rates of photocatalytic oxidation of organic carbon over illuminated titanium dioxide, J. Phys. Chem., 94 (1990) 6820–6825.

[32] S. Tamilselvi, M. Asaithambi, P. Sivakumar, Nano-TiO_2-loaded activated carbon fiber composite for photodegradation of a textile dye, Desal. Wat. Treat., 57 (2016) 15495–15502.

[33] D. Chen, A.K. Ray, Photocatalytic kinetics of phenol and its derivatives over UV irradiated TiO_2, Appl. Catal., B, 23 (1999) 143–157.

[34] C. Zhu, L. Wang, L. Kong, X. Yang, L. Wang, S. Zheng, F. Chen, F. MaiZhi, H. Zong, Photocatalytic degradation of azo dyes by supported TiO_2 + UV in aqueous solution, Chemosphere, 41 (2000) 303–309.

[35] W. Baran, E. Adamek, A. Makowski, The influence of selected parameters on the photocatalytic degradation of azo-dyes in the presence of TiO_2 aqueous suspension, Chem. Eng. J., 145 (2008) 242–248.

[36] S.H. Kim, H.H. Ngo, H.K. Shon, S. Vigneswaran, Adsorption and photocatalysis kinetics of herbicide onto titanium oxide and powdered activated carbon, Sep. Purif. Technol., 58 (2008) 335–342.

[37] J. Saien, S. Khezrianjoo, Degradation of the fungicide carbendazim in aqueous solutions with UV/TiO_2 process: optimization, kinetics and toxicity studies, J. Hazard. Mater., 157 (2008) 269–276.